

Foam Generation by Snap-off in Flow Across a Sharp Permeability Transition

Shah, S.Y.; As Syukri, Herru; Wolf, Karl-Heinz; Pilus, Rashidah M.; Rossen, Bill

DOI

[10.3997/2214-4609.201900147](https://doi.org/10.3997/2214-4609.201900147)

Publication date

2019

Document Version

Final published version

Published in

IOR 2019 20th European Symposium on Improved Oil Recovery

Citation (APA)

Shah, S. Y., As Syukri, H., Wolf, K.-H., Pilus, R. M., & Rossen, B. (2019). Foam Generation by Snap-off in Flow Across a Sharp Permeability Transition. In *IOR 2019 20th European Symposium on Improved Oil Recovery* Article We A 08 EAGE. <https://doi.org/10.3997/2214-4609.201900147>

Important note

To cite this publication, please use the final published version (if applicable). Please check the document version above.

Copyright

Other than for strictly personal use, it is not permitted to download, forward or distribute the text or part of it, without the consent of the author(s) and/or copyright holder(s), unless the work is under an open content license such as Creative Commons.

Takedown policy

Please contact us and provide details if you believe this document breaches copyrights. We will remove access to the work immediately and investigate your claim.

Green Open Access added to TU Delft Institutional Repository

'You share, we take care!' - Taverne project

<https://www.openaccess.nl/en/you-share-we-take-care>

Otherwise as indicated in the copyright section: the publisher is the copyright holder of this work and the author uses the Dutch legislation to make this work public.

We A 08

Foam Generation by Snap-off in Flow Across a Sharp Permeability Transition

S. Shah^{1*}, H. As Syukri¹, K. Wolf¹, R. Pilus², W. Rossen¹

¹Delft University of Technology; ²Universiti Teknologi PETRONAS

Summary

Foam reduces gas mobility and can help improve sweep efficiency in an enhanced oil recovery process. For the latter, long-distance foam propagation is crucial. In steady gas-liquid flow, foam is generated in homogeneous porous media by exceeding a critical pressure gradient, which normally only happens near the wellbore. Away from wells, these requirements may not be met, and foam propagation is uncertain.

It has been shown theoretically that foam can be generated, independent of pressure gradient, during flow across an abrupt increase in permeability. This could dominate foam generation away from wells in layered or laminated geological formations and can improve the chances of success of a foam application. The objective of this study is to validate theoretical explanations through experimental evidence and to quantify the effect of permeability contrast, velocity and fractional flow on this process.

In this study, we validate theoretical predictions through a variety of experimental evidence. Coreflood experiments involving co-injection of gas and surfactant solution at field-like velocities were performed. Layered, consolidated and well-characterized sintered glass cores were used as the porous media. The permeability change in each core was analogous to sharp, small-scale heterogeneities such as laminations and cross-laminations. The experiments were carefully designed not to allow foam generation by mechanisms other than snap-off at the permeability boundary in the core. Local pressure gradient was measured at various locations and was used to identify foam generation and subsequent propagation through the porous medium. Additionally, X-ray computed tomography (CT) was employed to detect changes in phase saturation that accompany foam generation and subsequent propagation downstream. CT-based saturations measurements were also used to qualitatively chart the reduction in capillary pressure across the sharp permeability jump, supporting theoretical explanations behind this process. The effect of permeability contrast, superficial velocity and flowing gas fraction on this process was also investigated. For a given permeability contrast, foam generation was observed at higher gas fractions than predicted by previous theory (Rossen, 1999). Conditions for propagation of foam were explored by successively performing experiments at lower velocities and higher gas fractional flows. Significant fluctuations in pressure gradient accompanied the process of foam generation, indicating a degree of intermittency in the generation rate - probably reflecting cycles of foam generation, dryout, imbibition, and then generation. The intermittency of foam generation was found to increase with decreasing injection velocities and greater permeability contrasts.

Introduction

Foams have numerous applications in the oil industry. They are used for drilling (Lyons et al., 2009), to divert acids in well-stimulation procedures (Chambers, 1994), for hydraulic fracturing in low-permeability formations (Gupta, 2009), to improve liquid lifting in low-pressure gas wells (Yang & Siddiqui, 1999) and for tertiary oil-recovery processes (Rossen, 1996). Foams are used to improve sweep in removing dense non-aqueous phase liquids (DNAPLs) in aquifer remediation applications (Hirasaki et al., 1997, 2000). In this work, we focus on the use of foam as a mobility-control agent in an enhanced oil recovery (EOR) process with an emphasis on capillary-dominated mechanisms of foam generation under low driving-force settings in porous media.

Most of the world's EOR production comes from injecting gases (Lake et al., 2014). Gas has a very low viscosity and density compared to oil, and, therefore, in a displacement process, sweep efficiency is poor due to viscous instability and gravity override. When applied as a dispersed phase, as in foam, its apparent mobility is greatly reduced and sweep efficiency is improved. In a heterogeneous, layered system, as discussed by Tanzil et al. (2002) and Shah et al. (2018), the effective permeability in the vertical direction may be greatly reduced by foam generation in the high-permeability strata, reducing the extent of gravity segregation.

There are three main mechanisms of creation of lamella (liquid films separating bubbles) in porous media: lamella division, snap-off, and "leave-behind" (Kovscek & Radke, 1994; Rossen, 1996), as shown in Figure 1. From the figure it can be inferred that, for lamella division to occur, one lamella or lens must be initially present. Leave-behind is prevalent when gas invades a liquid-filled medium, normally during a drainage process. Snap-off occurs due to a local reduction in capillary pressure that leads to the creation of a liquid bridge in the pore throat. Capillary pressure in the pore throat can be reduced in several ways (Rossen, 2003).

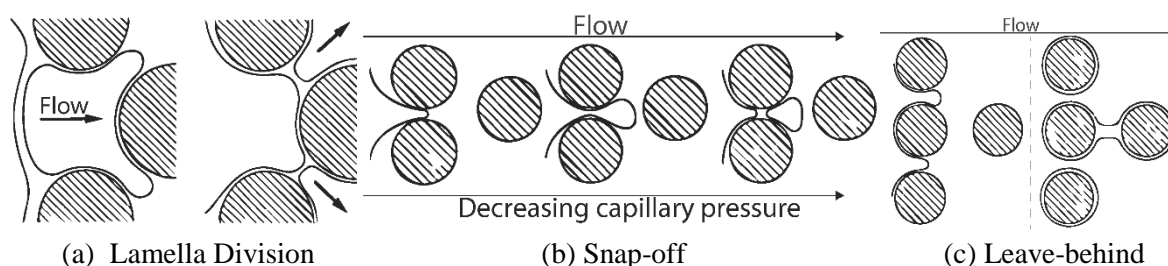


Figure 1 Primary mechanisms of lamella creation in porous media (Kovscek & Radke, 1994).

Numerous experimental studies (Gauglitz et al., 2002; Tanzil et al., 2002) and theoretical models (Friedmann et al., 1991; Kam & Rossen, 2003; Rossen & Gauglitz, 1990) suggest that in steady gas-liquid flow strong foam generation in porous media would require exceeding a critical pressure gradient or velocity threshold, which is typically only overcome in the near-well region. Creation of foam in these cases is thought to depend either on mobilization of lenses and lamellae and subsequent lamella division or on the increased frequency of snap-off as a function of local pressure gradient or flux. Away from wells, pressure gradient is low and the darcy velocity is considered to be approximately 1 ft/d (Dake, 1994); much lower than the reported thresholds. Therefore, it is uncertain whether foam can propagate long distances away from wells where the critical requirements for creating new lamellae and sustaining foam may not be satisfied (Ashoori et al., 2012; Friedmann et al., 1994; Yu et al., 2018). This work concerns snap-off in flow of gas and surfactant solution across a sharp increase in permeability (Falls et al., 1988; Hirasaki et al., 2000; Li & Rossen, 2005; Shah et al., 2018; Tanzil et al., 2002), which is theoretically shown to be independent of pressure gradient (Rossen, 1999). Therefore, this mechanism can cause foam generation away from wells and can assist in long-distance foam propagation, thereby improving overall sweep efficiency in a subsurface foam application.

Sharp heterogeneities are quite common in petroleum reservoirs and shallow aquifers. They exist over a wide range of length scales. The most prevalent are unconformities such as sharp layer boundaries, which can extend from a few metres to several hundreds of metres in length (Reineck & Singh, 1980). Layered systems often consist of internal laminations that add to the frequency of sharp changes in permeability in a given rock volume. Cross-laminations present abrupt permeability contrasts in the horizontal direction (Hartkamp-Bakker, 1993), offering locations for foam generation by snap-off during lateral pressure-driven flow.

In multiphase flow across an abrupt increase in permeability, the wetting phase accumulates upstream of the permeability change as a result of capillary continuity across the transition (Yortsos & Chang, 1990). The extreme case of this phenomenon occurs at the outlet of the core as the so-called capillary end effect. As a result, local capillary pressure is reduced immediately upstream of the permeability contrast. If the capillary pressure falls below the critical capillary pressure for snap-off, i.e. P_c^{sn} , snap-off, and, consequently, foam generation, can be expected. The ratio of capillary entry pressure (P_c^e) to P_c^{sn} is dependent on the pore geometry. Falls et al. (1988) measured P_c^{sn} for beadpacks, which are reasonable representations of conventional reservoir rocks, and found that $P_c^{sn}/P_c^e \approx 1/2$. Rossen (1999) used this result to show that for snap-off to occur in flow from low- to high-permeability formations, capillary pressure in the high-permeability zone must be less than half the capillary pressure in the low-permeability zone ($P_c^H < P_c^L/2$). In other words, the high-permeability region must be at least four times as permeable as the low-permeability region ($k^H \geq 4 k^L$), assuming $P_c \propto \sqrt{1/k}$. As the flow gets drier, a greater permeability contrast may be required to cause foam generation. Figure 2 shows the calculations of Rossen (1999), where the permeability contrast required to block gas flow by snap-off (effectively causing foam generation) is plotted as a function of the gas-water relative-permeability ratio far from the transition zone in the absence of foam. The relative-permeability ratio relates to the injected fractional flow, as $f_w = [1 + (k_{rg}/k_{rw})^0(\mu_w/\mu_g)]^{-1}$. Therefore, if $f_g = 80\%$ and $\mu_w/\mu_g = 50$, $(k_{rg}/k_{rw})^0 = 0.08$. According to Figure 2, a permeability jump slightly higher than 4, at $f_g = 80\%$, would cause foam generation, independent of velocity or pressure gradient. However, if the pore geometry deviates from a circular shape, the ratio of $P_c^{sn}/P_c^e \approx 1/2$ may be larger or smaller than 1/2 (Chambers & Radke, 1990; Lenormand et al., 1983; Rossen, 2003). As a result, a greater or lower permeability contrast, respectively, may be required to block gas flow by snap-off at the same flowing gas fraction. It is important to note that while capillary pressure falls at the edge of the low-permeability zone, gas bubbles are expected to form at the entrance to the high-permeability zone. There is no dependency on pressure gradient. However, mobilisation of the bubbles and subsequent propagation away from the heterogeneity would require such a driving force.

As mentioned above, experimental examination of foam generation across permeability contrasts has been carried out in the past. However, previous studies were either conducted using porous media with a very large permeability contrasts (far from the threshold) or were conducted under drainage conditions where other mechanisms of foam generation may dominate. In this work, the experiments were carefully designed not to allow foam generation by mechanisms other than snap-off at the permeability boundary. A series of experiments were performed over a wide range of experimental conditions examining the effect of fractional flow, velocity and permeability contrast on this phenomenon. The experimental conditions used in this study were closer to those encountered in a deep reservoir setting, compared to previous work. Additionally, we utilise an artificial, well-characterized and consolidated porous medium compared to unconsolidated sandpacks in earlier research. Falls et al. (1988) conducted their experiments in sandpacks with permeability contrasts of 20:1 and higher. The lowest total superficial velocity in their experiments is 0.51 cm/min (~24 ft/d). As a result, the velocity in the porous medium is more representative of the near-well region and not deep inside the reservoir, where this mechanism is most likely to be dominant and impact the efficiency of a foam application. Tanzil et al. (2002) observed foam generation in their sandpack across a permeability contrast of approximately 4.4:1 at approximately 0.9 ft/d (gas velocity = 0.6 ft/d). However, they conducted their experiments under drainage conditions by injecting gas and surfactant solution into a surfactant-saturated medium. As discussed above, under drainage conditions, other mechanisms of foam generation such as Roof snap-off and leave-behind are known

to cause foam generation. Li & Rossen (2005) did not observe foam generation during simultaneous injection of gas and surfactant solution into a sandpack across a permeability contrast of approximately 4:1, contrary to the theory of Rossen (1999). They suspected that gas bypass along the edges of the pack because of imperfect packing might have been the reason for failing to observe foam generation. They did, however, report foam generation across a permeability contrast of 20:1 at a velocity of 2.14 ft/d. The mobilization of this foam was periodic.

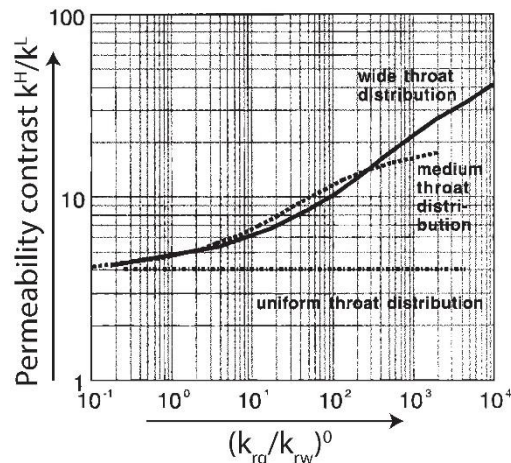


Figure 2 Theoretically computed permeability contrast required to completely block gas flow as a function of gas-water relative permeability ratio $\left(\frac{k_{rg}}{k_{rw}}\right)^0$, with the superscript denoting its value far from the transition zone (Rossen, 1999). Left to right on the x-axis also represents an increase in gas fraction, as $f_w = \left[1 + \left(\frac{k_{rg}}{k_{rw}}\right)^0 \left(\frac{\mu_w}{\mu_g}\right)^{-1}\right]^{-1}$.

In this work, we follow an experimental procedure similar to the work of Li & Rossen (2005). Foam-generation experiments are conducted by co-injecting surfactant solution and gas at field-like velocities, in a consolidated sintered-glass porous medium with two layers perpendicular to the direction of flow. An important objective of this work is to validate the theoretical predictions of foam generation (Rossen, 1999) through coreflood experiments that isolate snap-off resulting from a capillary pressure contrast as the only lamella-creation mechanism. Local pressure gradient and saturation maps obtained through X-ray computed tomography (CT) are the primary measurements used to identify foam generation and mobilisation. Pressure gradient is used to quantify foam strength, whereas local saturation near the permeability contrast is used to quantify the reduction in capillary pressure that causes foam generation. A variety of injection rates and injected gas fractions are employed to validate the threshold conditions for foam generation.

The paper is structured as follows. The next section describes the experimental set-up and procedure followed. Next, under “Results”, the outcome of different foam-generation experiments is reported. Under “Discussion”, an analytical examination of these results is followed and the main conclusions of this work are presented in final section.

Experimental Methodology

The materials used in this study, together with the experimental protocols followed, are identical to those described by Shah et al. (2018). Nevertheless, we highlight important aspects of the same to ensure an independent readability of this manuscript.

Materials and Chemicals

We conduct coreflooding experiments with co-injection of gas and surfactant solution into a synthetic porous medium made from sintered borosilicate glass. The cores were acquired from Hilgenberg GmbH, Malsfeld, Germany (www.hilgenberg-gmbh.de) and were prepared by sintering crushed, pure

borosilicate glass. The cores were roughly 40 ± 2 cm long with a diameter of 3 ± 0.1 cm. Each core has a single sharp and monotonic jump in permeability roughly one-third of the way along the length of the core. In other words, roughly one-third of the core comprised a homogeneous low-permeability section whereas the rest formed the homogeneous high-permeability zone. The permeability change is achieved by sintering different grain sizes in the same core. The glass grains are angular, as can be seen in the picture on the right in Figure 3. Four different core samples are used in this study to probe the effect of permeability contrast on foam generation by snap-off. The details of the cores are outlined in Table 1. In order to examine the effect of velocity and fractional flow on foam generation, core 1 was utilized and the injected gas fraction and velocity was systematically varied. In core 1, the low-permeability section has a measured permeability (k^L) of 5.4 ± 0.02 D, whereas the high-permeability section has a permeability (k^H) of 20.7 ± 0.2 D. Therefore, the permeability contrast ($\langle k^H/k^L \rangle$) is roughly 3.8:1, bordering the threshold predicted by Rossen (1999).

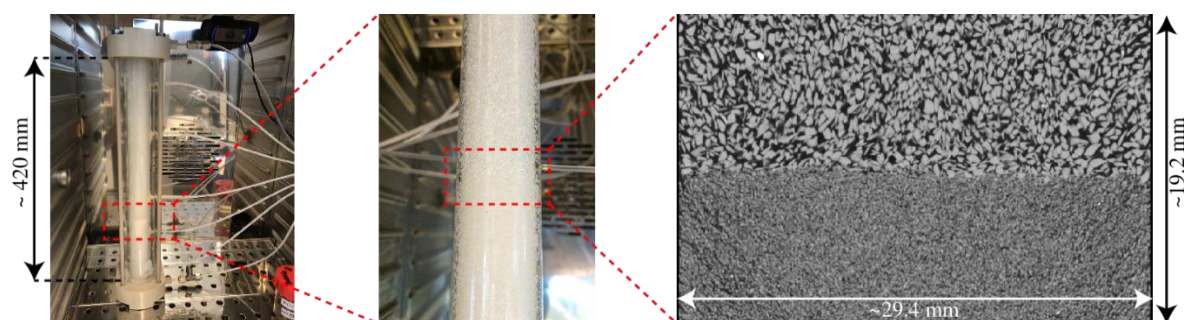


Figure 3 Core holder (left) with a synthetic sintered-glass core (left and center) and a μ CT image of a vertical cross-section near the permeability contrast in the core (Shah et al., 2018).

Anionic alpha olefin sulphonate (AOS) C_{14-16} with a molecular weight of 315 g/mol (Stepan BIO-Terge[®] AS-40 KSB) was used as the foaming surfactant. 99.98% N_2 is used as the gas phase and the surfactant solution comprises 0.5 wt.% (≈ 0.04 M) surfactant and 1 wt.% (≈ 0.17 M) NaCl in each foam generation experiment. For a variety of reasons including cost, detergency and low adsorption on sandstones, AOS is an excellent overall candidate for foam enhanced oil recovery in a conventional, mature oil reservoir (Farajzadeh et al., 2008).

Table 1 Details of core samples used, highlighting absolute permeability of individual sections.

Core sample	Pore Size specified by manufacturer (μ m)	Approximate pore volume (ml)	Permeability (darcy)	$\langle k^H/k^L \rangle$
1	Low perm: 16-40 μ m High Perm: 40-100 μ m	99	Low perm (k^L): 5.4 ± 0.02 High Perm (k^H): 20.7 ± 0.2	3.8
2	Low perm: 40-60 μ m High Perm: 100-160 μ m	99	Low perm: 10.9 ± 0.01 High Perm: 59.3 ± 0.8	5.4
3	Low perm: 16-40 μ m High Perm: 100-160 μ m	80	Low perm: 3.1 ± 0.01 High Perm: 43.2 ± 0.2	13.9
4	Low perm: 16-40 μ m High Perm: 100-160 μ m	96	Low perm: 1.7 ± 0.15 High Perm: 46.7 ± 2.0	27.5

Experimental Procedure

Every experiment begins with multiple permeability measurements using water across the length of the core to ensure that there has been no grain migration and that there is no trapped gas in the core. Next, the core is saturated with brine solution (1 wt.% NaCl prepared in demineralized water) and the permeability is measured again. The permeability to water and brine is determined from the slope of the straight line formed by a plot of superficial velocity vs. the ratio of pressure gradient measured across the two core sections to viscosity (i.e. q/A vs. $\nabla P/\mu$). The confidence interval for estimating this slope is reported Table 1 in darcies. Once the core is saturated with brine, the flow rate is reset to the desired experimental value and gas is co-injected at the desired fractional flow. When gas-brine

co-injection reaches steady-state, surfactant solution replaces the brine solution. Once the surfactant front reaches the permeability transition, foam generation is expected. The core is cleaned thoroughly after each experiment by flushing with 50 wt.% iso-propanol solution for several pore volumes followed by a similar amount of demineralized water. Trapped gas is displaced out of the core by injecting several pore volumes of CO₂. This eliminates any chances of hysteresis effects affecting the foam-generation experiments (Kahrobaei et al., 2017).

Experimental Apparatus

Figure 4 shows a schematic flow diagram of the experimental set-up. While Figure 3 shows the core in a vertical orientation, when in the dual-beam CT scanner the core is placed horizontally. This is not ideal for flow behaviour but is necessary in order to minimize the impact of beam-hardening effects and cross-artefacts while taking CT scans of a non-axisymmetrically placed object. Therefore, gravity segregation affects the experiments conducted using the CT scanner, as discussed by Shah et al. (2018). Along with saturation maps obtained through CT scans, pressure measurements in the low-permeability section are used to confirm that no foam is generated before the permeability contrast. In order to avoid fluctuations caused by multiphase flow through the back-pressure regulator assembly, no back-pressure is applied and the outlet of the core is open to atmospheric pressure. Such fluctuations may cause foam generation (Li & Rossen, 2005). The entire apparatus is placed on top of the CT scanner table for experiments where phase saturations are measured. The medical CT scanner is housed in a temperature-controlled room at 21±0.4 °C.

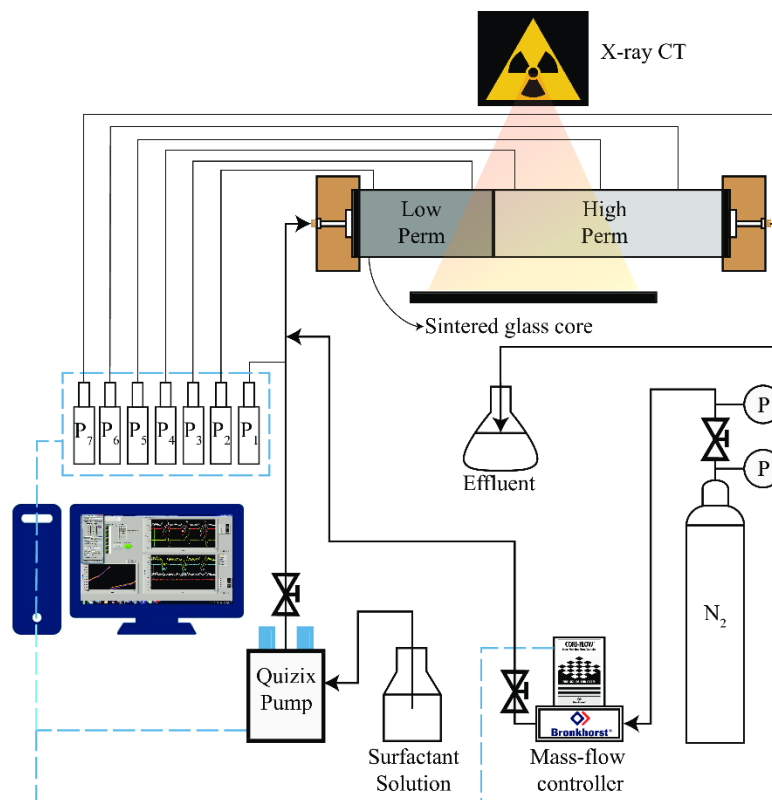


Figure 4 Schematic of the experimental set-up (Shah et al., 2018).

CT image acquisition and processing

The Siemens SOMATOM Definition Dual Energy CT scanner was used to scan the core in select experiments, in order to quantify phase saturations through the course of the experiment. A single-energy X-ray beam was sufficient when scanning because the experiments involved two-phase flow of fluids differing greatly in density. An overview of the applied image settings is reported in Table 2. Single-slice helical CT scans were acquired with a pitch of 0.9. A pitch less than 1.0 ensures X-ray beam overlap for the same scanned volume, resulting in a better image quality. The lower the pitch, greater the scan time. These image settings resulted in approximately 260 slices for each scan along

the axis of a core, taken over a period of approximately 9 seconds. One slice contains 512×512 pixels, a part of which contains the circular core cross-section. The images obtained were further processed to compute phase saturations using Fiji (Schindelin et al., 2012), a distribution of the ImageJ software.

Table 2 Settings applied to the CT scanner.

Parameter	Setting
Tube Voltage	140 KeV
Tube Current	250 mA
Pitch	0.9
Slice thickness	1.5 mm
Pixel size	$1.5 \times 1.5 \text{ mm}^2$
Scan mode	Spiral

Raw CT data in terms of Hounsfield units (HU) are used to compute porosity and phase saturations as a voxel property for each image stack. Porosity can be obtained using the CT scans of a dry and water-saturated core (Mees et al., 2003). During the course of the experiment, liquid-phase saturation is computed for each scan as:

$$S_w = \frac{HU_{\text{exp}} - HU_g}{HU_w - HU_g} \quad (1)$$

where HU_{exp} denotes the CT measurement taken during the course of the multiphase flow experiment. HU_g is the CT measurement of a dry core, obtained when the core is not yet saturated with any liquid, before each experiment. HU_w represents the CT measurement for a core that is fully saturated with the liquid phase. In this work, HU_w is recorded before the start of each experiment, when the core is fully saturated with brine solution. It is important to note that the accuracy of CT measurements depends on different parameters selected for the X-ray source, such as applied beam voltage, corresponding beam energy and the applied filters for shaping the beam. Once the liquid phase saturations are computed for each multiphase scan, a colour scheme is applied to the images, where blue represents the aqueous phase and red represents the gas phase. The images are cropped to include only the circular cross-section of the core; phase saturation maps from select experiments are shown in the next section. The saturation profile across the core can also be obtained by averaging values within each cylindrical image slice. This is also shown for select experiments in the next section and is used to quantify the local reduction in capillary pressure at the edge of the low-permeability zone in the “Discussion” section.

Results

A series of experiments were performed to examine the impact of permeability contrast, gas fraction and velocity on foam generation across a sharp increase in permeability and subsequent mobilisation. Injection conditions were systematically varied with core 1 ($k^H/k^L \approx 3.8:1$) for the last two. Foam generation was observed in all the experiments performed and reported in this paper.

Effect of velocity

Total injection rates were varied in a descending order from 0.1 ml/min to 0.025 ml/min (with steps of 0.025 ml/min), which translates to a total superficial velocity ranging from 0.67 ft/d to 0.17 ft/d, respectively. Gas fractional flow was fixed at 80%. Foam generation was observed at all the tested velocities. However, differences in foam propagation away from the permeability transition were seen in terms of changes in local pressure gradient. Figure 5b shows a typical measurement of pressure gradient across various sections of the core indicated in Figure 5a. The maximum pressure drop across

the core in all experiments is close to 0.5 bar and the outlet of the core is at atmospheric pressure. Figure 5b reports pressure gradient for the experiment conducted at $u_t = 0.5$ ft/d, whereas Figure 5c reports the experiment conducted at the lowest velocity, i.e. $u_t = 0.17$ ft/d. The horizontal axis represents total pore volumes of surfactant solution and N_2 gas injected (PVI). The core has reached a steady-state to gas-brine injection at the origin of the plot.

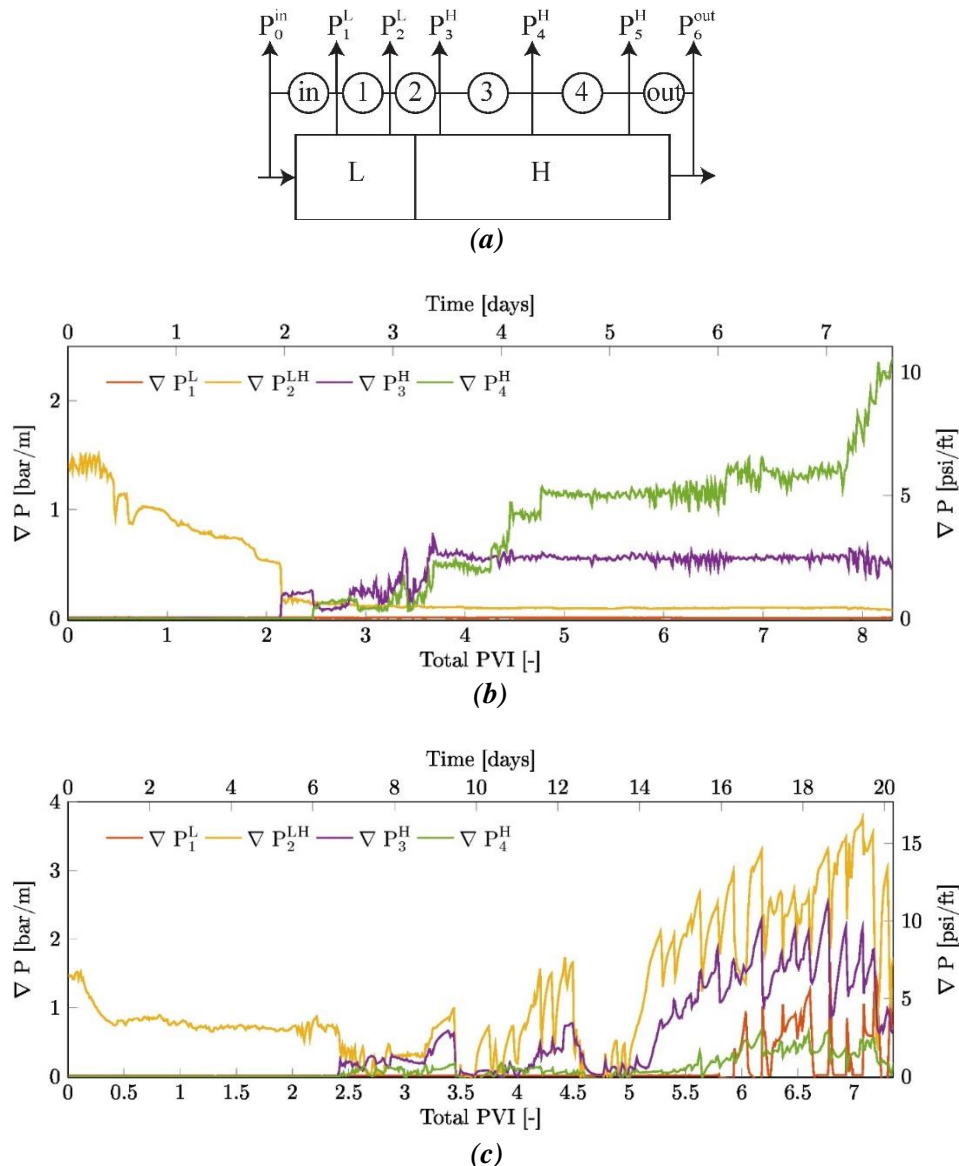


Figure 5 Schematic of core showing labelling scheme used to denote absolute pressure and pressure gradient (a); Pressure gradient across various sections of the core during the foam-generation experiment conducted at $u_t=0.5$ ft/d (b) and $u_t=0.17$ ft/d (c) at a fixed gas fractional flow of 80%. Superscript L represents a measurement in the low-permeability section, whereas superscript H represents data acquired from the high-permeability zone. LH represents the interval with the boundary.

As mentioned above, before surfactant is introduced in the core, each experiment starts with gas injection into a brine-saturated core. As gas drains the low-permeability section, the pressure transducers report a jump in pressure, indicating the arrival of gas. If each transducer measures the same phase once gas has arrived at the outlet of the core, then these jumps in absolute pressure correspond to spikes in terms of pressure gradient. However, in all the experiments conducted, regardless of the orientation of the core, the pressure gradient across the permeability transition ∇P_2^{LH}

(yellow line in Figure 5) is atypically high for gas-brine injection and the pressure gradient immediately downstream ∇P_1^L registers a slightly negative value. We believe that this is due to the pressure tap right before the permeability transition sensing a different phase compared to the rest of the ports (McCool et al., 1983; Shah et al., 2018). Gas trapping and the capillary-pressure contrast within the core may add to this effect. The experimental data reported by As Syukri (2018) during gas-brine flow for similar experiments further supports this explanation. As more and more surfactant is injected, ∇P_2^{LH} gradually declines. When the surfactant arrives at the permeability contrast, foam is generated across the permeability transition. As the foam strength increases, the pressure taps in the high-permeability zone sense the reduction in gas mobility starting with the transducer immediately downstream of the transition. This is represented by the sharp drop in ∇P_2^{LH} , and jump in ∇P_3^H , at about 2.2 total PVI (0.44 PVI liquid) in Figure 5b and 2.4 total PVI (0.4 PVI liquid) in Figure 5c. ∇P_4^H rises shortly thereafter. In Figure 5b, ∇P_4^H rises further later in the experiment, at around 4.5 PVI total. This corresponds to the passage of foam across the final section in the high-permeability zone followed by its arrival at the outlet of the core.

It is important to note that the pressure gradient in the low-permeability zone ∇P_1^L is low and does not indicate any reduction in gas mobility due to foam generation upstream of the permeability jump. Evidently, the magnitude of pressure fluctuations downstream of the jump increases at lower injection velocities. We term this the intermittency of foam generation; it is discussed in more detail through the paper. For the foam-generation experiments conducted at $u_t = 0.67$ ft/d, $u_t = 0.5$ ft/d (Figure 5b) and $u_t = 0.33$ ft/d, pressure gradient in the final section inside the high-permeability zone, ∇P_4^H , is either similar to or greater than ∇P_3^H in magnitude. In these experiments, the strength of foam generated at the permeability transition is maintained as it propagates downstream to the outlet of the core. However, as shown in Figure 5b, at $u_t = 0.17$ ft/d, ∇P_4^H is lower than ∇P_3^H , indicating a drop in foam strength upon propagation. At this velocity, we reach the limit of foam propagation and the foam generated at the permeability contrast is unable to steadily reach the outlet of the core. This is confirmed by observations made in the immediate vicinity of the outlet of the core (Figure 6). A typical observation made at the outlet of the core is shown in Figure 6a for $u_t = 0.5$ ft/d. At this velocity (and higher velocities), steady foam production is observed with infrequent, short, intermittent alternating bursts of gas and liquid production. At $u_t = 0.17$ ft/d, however, short periods (few minutes to an hour) of relatively coarse foam production is observed (Figure 6b) followed by a large amount of gas production (several hours to a day, corresponding to a few PVI), followed by liquid for a similar time interval. Differences in foam texture were also witnessed in the outlet tubing.

Snap-off in flow of gas and surfactant solution across an abrupt heterogeneity is intermittent in nature (Falls et al., 1988; Shah et al., 2018). Foam is not created steadily across the interface as surfactant solution reaches the permeability jump. Instead, in our experiments, the onset of foam generation, and often the period thereafter, is accompanied by large fluctuations in measured pressure gradient across the permeability transition and in the high-permeability zone. As mentioned earlier, foam generation begins when capillary pressure at the edge of the low-permeability zone falls below P_c^{sn} . Snap-off in pore throats blocks the flow of gas causing the local gas fraction to increase and the flow to become drier. Locally, the capillary pressure may momentarily rise above P_c^{sn} and foam generation stops. Eventually, liquid convects or imbibes back to the boundary of the low-permeability zone and accumulates, creating favorable conditions for snap-off. This cycle of events repeats itself and in combination with periodic plugging and mobilization of fluids at the boundary due to foam generation, it is responsible for the large fluctuations in pressure gradient observed in our experiments. We observe that this intermittency, in terms of magnitude and frequency of fluctuations in pressure gradient, is greater as the velocity decreases. Figure 7 shows the measured pressure gradient across the entire high-permeability zone (Figure 7a) and the corresponding apparent viscosity (Figure 7b). Apparent viscosity is computed as $\mu_{app}^H = (k^H \nabla P^H) / u_t$ where k^H is the measured permeability in the high-permeability section, ∇P^H is the pressure gradient across the same section during the experiment and u_t is the total superficial velocity. Each data point represents all the measurements recorded and averaged over 0.05 PVI of surfactant solution (or 0.25 total PVI). The

error bar in each direction represents one standard deviation of all the measurements within this window, representing the magnitude of fluctuation in pressure gradient. As the injection rate decreases, the magnitude of these fluctuations increases. For each case, the pressure gradient rises after roughly the same amount of liquid injected (≈ 0.4 PV), corresponding to the time at which the surfactant solution arrives at the permeability contrast.

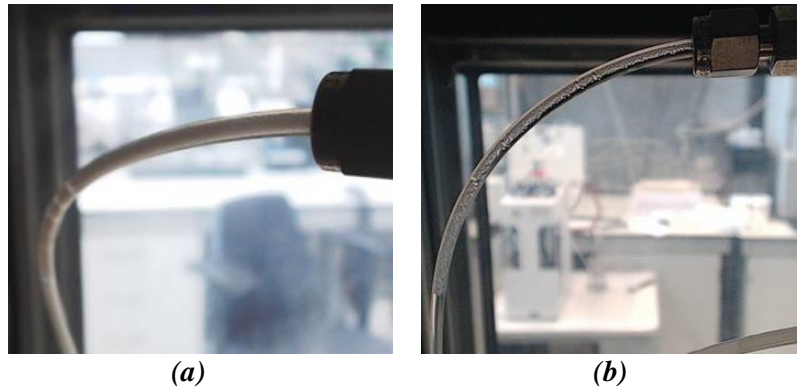


Figure 6 Snapshots of the outlet tubing showing fluids produced from the core as a typical observation of steady foam production at $u_t = 0.5$ ft/d (a). At $u_t = 0.17$ ft/d, short bursts of foam production preceded by liquid (b), followed by a few pore volumes of gas production, followed by liquid, is observed.

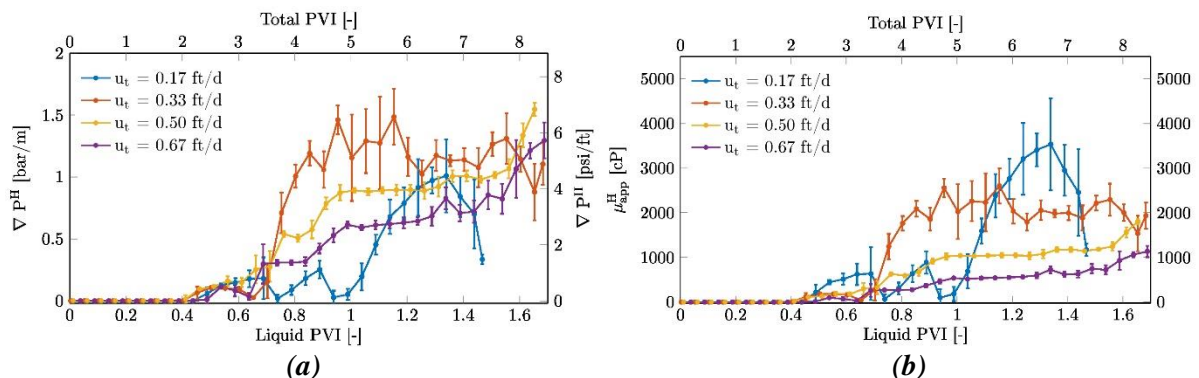


Figure 7 Pressure gradient measured across the high-permeability section of the core at four different injection rates (a) and corresponding apparent viscosity (b). $f_g = 80\%$ in all the experiments.

Effect of fractional flow

Injection rate was fixed and gas fraction was varied in experiments conducted using core 1 to examine the effect of fractional flow on foam generation across a sharp permeability contrast. Figure 8 shows two foam-generation experiments performed at the same injection rate but with different fractional flow. The core has been placed horizontally on the medical CT scanner table. Figure 8a shows pressure gradient versus pore volumes injected at $u_t = 0.67$ ft/d and $f_g = 60\%$. The lower horizontal axis represents pore volumes of surfactant solution injected into the core. Close to around 1 PVI total or 0.4 PVI liquid, foam generation takes place across the permeability transition, indicated by the drop in ∇P_2^{LH} and jump in ∇P_3^H , similar to the experiments reported above. The dashed lines in the plot indicate times at which CT scans were taken across the core. Phase saturations in each voxel of the CT image stack are computed using these scans, as explained earlier. In Figure 9, average liquid-phase saturation as seen in a vertical cross-section through the centre of the core is shown, with the pore volumes of liquid injected indicated on the left corresponding to dashed lines in Figure 8a. In the image at 0.5 PVI surfactant solution, gas saturation begins to rise in the high-permeability zone immediately downstream of the permeability transition. This confirms that the drop in ∇P_2^{LH} and jump in ∇P_3^H mark the onset of foam generation across the permeability contrast. At the start of surfactant injection, we observe an ambiguous build-up in gas saturation near the inlet of the core, as seen in the

image at 0.08 PVI liquid. However, this does not correspond to a reduction in gas mobility in terms of pressure gradient as there is no evident rise in ∇P_1^L (red line in Figure 8a). This region of high gas saturation does not appear in subsequent CT images, confirming that foam is indeed generated at the permeability transition, seen clearly as a sharp contrast in gas saturation across the boundary in the CT images. There is no strong foam present in the low-permeability zone. After 1.2 pore volumes of surfactant injection, foam has propagated downstream from the permeability contrast to the final section in the high-permeability region and ∇P_4^H gradually rises. The experiment is ended shortly after 2.2 PVI liquid as foam arrives at the outlet of the core. Figure 10 shows the liquid-saturation profile for the same experiment plotted against a dimensionless distance along the core, where each point represents an average value in the circular image slice at that position.

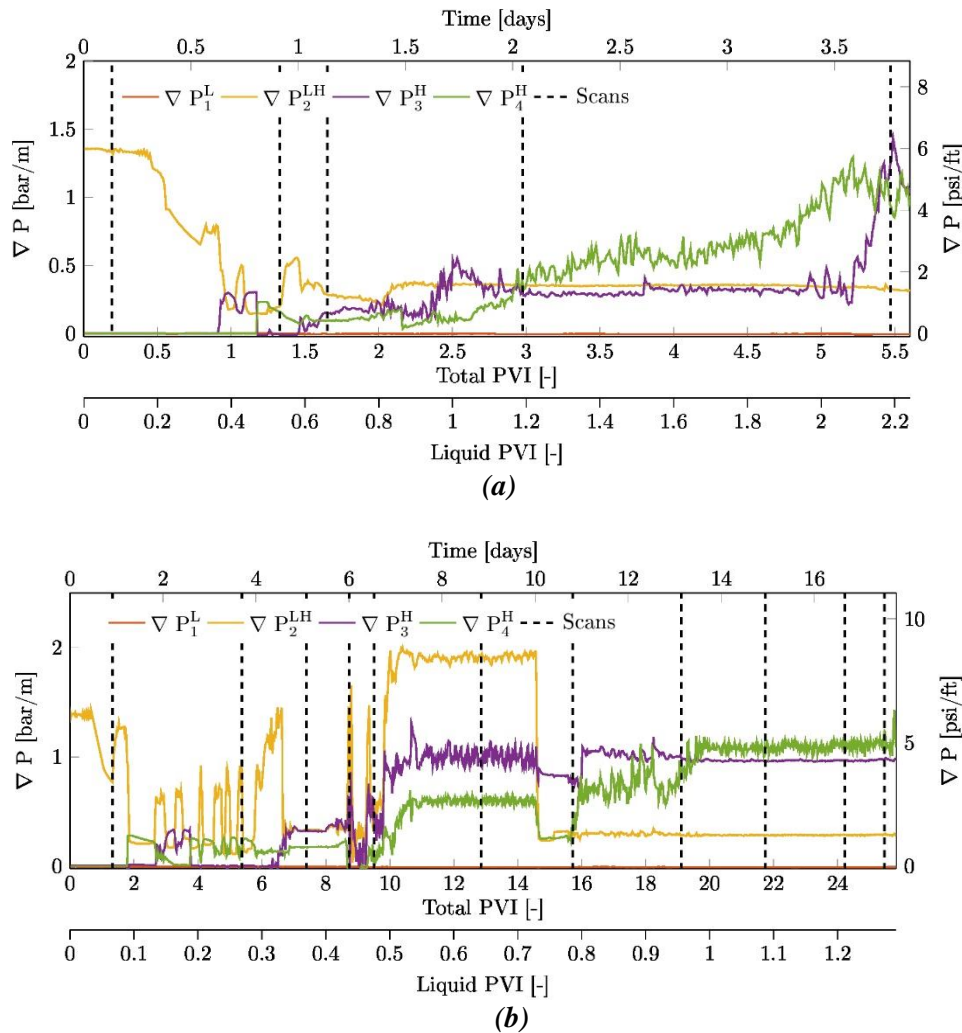


Figure 8 Pressure gradient across various sections of the core plotted against both total and surfactant (secondary horizontal axis) pore volumes injected during the foam-generation experiment conducted at $f_g=60\%$ (a) and $f_g=80\%$ (b) at a fixed total superficial velocity of 0.67 ft/d. Superscript L represents a measurement in the low-permeability section, whereas superscript H represents data acquired from the high-permeability zone. LH represents the interval with the boundary.

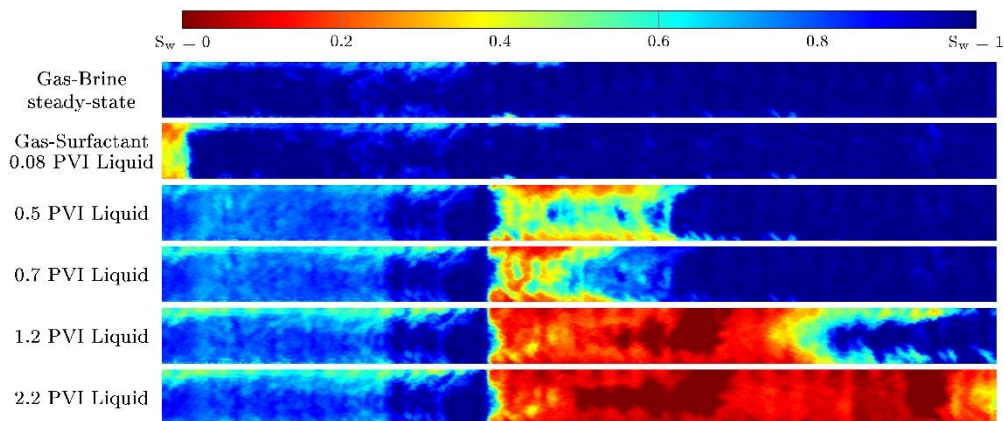


Figure 9 Average liquid-saturation in a vertical cross-section through the center of the core obtained using X-ray CT imaging for the foam-generation experiment conducted at $u_t = 0.67$ ft/d and $f_g = 60\%$. The image at the top represents a measurement during steady-state gas-brine co-injection and the images thereafter were taken at times corresponding to dashed lines in Figure 8a. Blue represents a high liquid saturation whereas red represents a high gas saturation, as indicated by the color bar at the top.

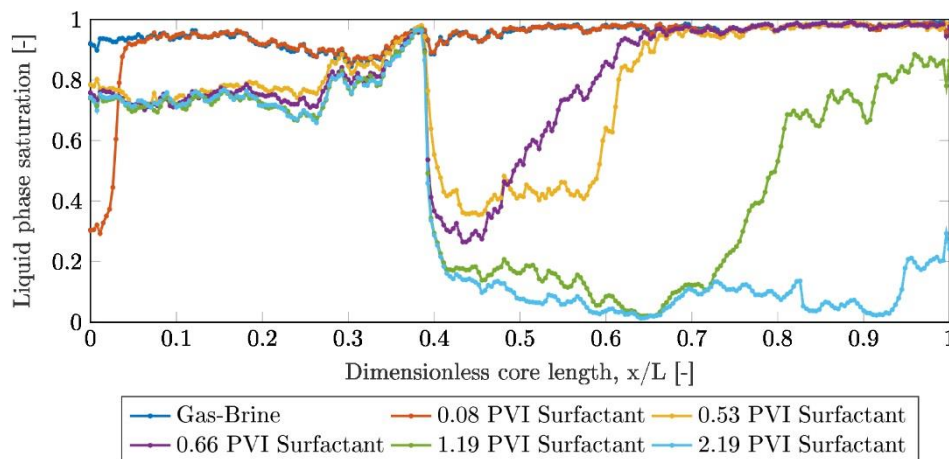


Figure 10 Average liquid-phase saturation profile in the core corresponding to the experiment shown in Figure 8a and Figure 9. Each point represents an averaged saturation in a circular slice at the corresponding location in the core.

Figure 8b shows pressure gradient versus pore volumes of injection for an experiment performed at the same injection rate ($u_t = 0.67$ ft/d) but a higher injected gas fraction ($f_g = 95\%$). Figure 11 reports phase saturations for this experiment, computed using X-ray CT imaging and averaged to a single value in each cylindrical image slice. Evidently, pressure gradient across the permeability transition exhibits larger fluctuations in this case and foam arrives at the outlet faster (in terms of liquid injected) compared to the experiment conducted at $f_g = 60\%$. At roughly 0.1 pore volumes of surfactant injection, pressure gradient in the high-permeability zone appears to rise. In this case, however, this response does not mark the onset of foam generation, as the saturation profile corresponding to 0.27 PVI liquid (yellow line in Figure 11) does not indicate foam in the high-permeability zone (gas saturation is comparable to gas-brine steady-state). The next saturation profile, at 0.37 PVI liquid, shows a foam front (in terms of a high gas-saturation) propagating through the high-permeability zone. Therefore, the onset of foam generation is in fact marked by the sharp drop in ∇P_2^{LH} and rise in ∇P_3^H at approximately 0.33 pore volumes of surfactant injection. Gas saturation in the low-permeability region increases substantially after surfactant is introduced in the core. The saturation profile at 0.48 PVI liquid and 0.64 PVI liquid show a gas saturation of almost 85% in the low-permeability zone, close to the permeability transition. Later in the experiment, the gas saturation

is lower, at about 60%. The relatively high gas saturation, however, does not correspond to a significant reduction in gas mobility, as ∇P_L^L stays low. Pressure drop in the low-permeability section gradually rises from about 1 mBar to 10 mBar through the experiment. The absolute pressure transducers are accurate upto 3 mBar. This allows for a maximum mobility reduction by a factor of 16. We think that the relatively high gas saturation in the low-permeability zone, in this experiment, is due to the creation of a continuous-gas foam. If the foam were discontinuous, blocked flow-paths and moving lamellae would register a higher pressure gradient (and consequently, a higher mobility reduction factor) in the low-permeability section, closer to the measurements in the high-permeability zone. Moving lamellae would multiply by lamella division and this would abruptly increase pressure gradient as the experiment progressed. Thus, it is a continuous gas phase, without moving lamellae, that reaches the permeability transition. Nevertheless, strong foam is generated in flow across this jump in permeability and the foam propagates downstream from the heterogeneity towards the outlet of the core.

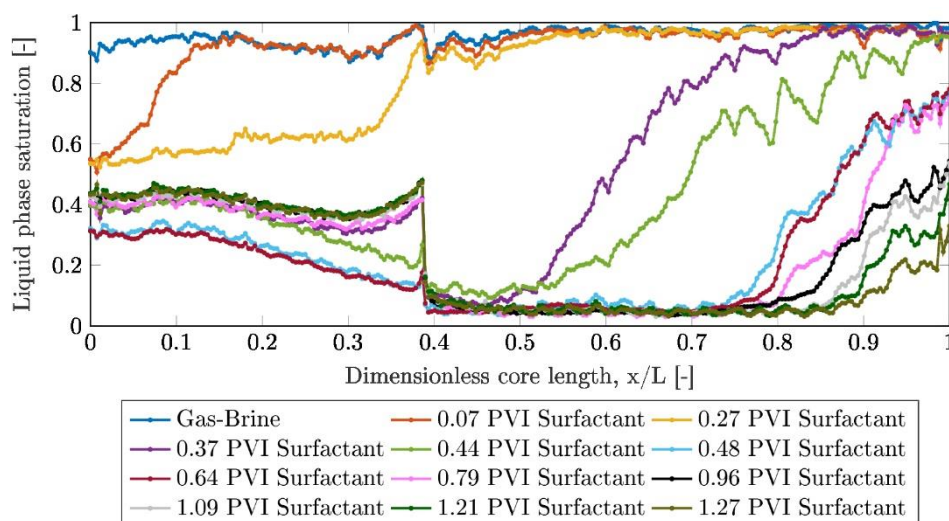


Figure 11 Average liquid-phase saturation profile in the core corresponding through the course of the experiment shown in Figure 8b. Each point represents an averaged saturation in a circular slice at the corresponding location in the core.

In both the experiments reported in Figure 8, foam generation takes place after similar amounts of liquid injection, which conforms with the expected time of arrival of the surfactant solution at the permeability contrast. However, the pressure response to the same is quite different. Pressure gradient across the permeability contrast exhibits large fluctuations at $f_g = 95\%$. As mentioned above, when looking at the pressure measurements, it appears that a modest and arguably sporadic resistance to gas flow is witnessed in the high-permeability zone long before foam begins to appear in the CT images as a high-gas-saturation front moving through the region. At the end of both experiments, pressure gradient in the high-permeability zone is similar at around 1 bar/m. This indicates minimal to no sensitivity of the final mobility to the change in fractional flow. Experiments conducted at other gas fractions, as reported in the next section, also yielded similar observations. The theory of Rossen (1999) suggests that foam generation is easier in wetter flow. However, we do not observe significant differences in foam strength and the time at which foam generation commences at lower gas fractions to support this idea. For a permeability contrast of approximately 3.8:1, foam generation is observed at higher gas fractions than predicted by theory (Figure 2).

Effect of permeability contrast

Four different core samples (Table 1) were used to perform foam-generation experiments at a fixed total injection velocity of 0.67 ft/d and injected gas fraction of 80%, in order to observe the effect of changing permeability contrast. On average, this translates to about 1.4 PV/day of total fluid injection for each core. Foam was generated across the permeability transition in all the experiments. Figure 12 shows the results of four experiments with apparent viscosity of foam in the high-permeability section

plotted against total and liquid pore volumes of injection. Each point represents measurements recorded over a period of 0.05 liquid PVI (or 0.25 total PVI). The error bar represents the spread of the data acquired in this time period, indicating the fluctuating nature of pressure gradient through the foam-generation experiment. The average apparent viscosity of foam generated across a sharp permeability increase, ranges from about 600 cP to 1800 cP, with the highest apparent viscosity recorded towards the end of the experiment with core 4 at approximately 2750 cP. Evidently, the greater the permeability contrast in the core, the larger the apparent viscosity of the generated foam. Additionally, at a greater permeability contrast, it takes longer to observe foam in the high-permeability section, especially in the core with the greatest permeability contrast (purple line Figure 12). We think that this might be due to a greater intermittency in foam generation, as explained earlier, across greater permeability contrasts.

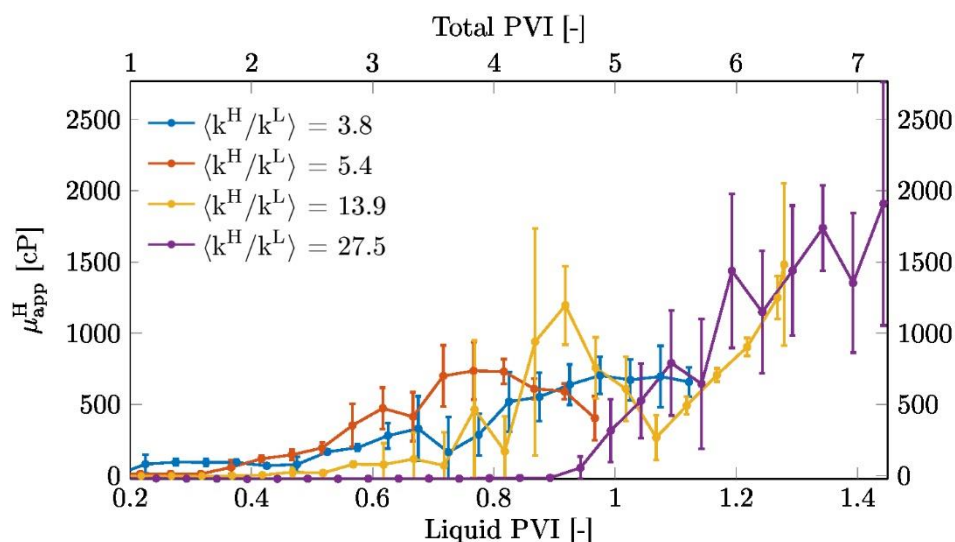


Figure 12 Apparent viscosity of foam in the high-permeability region of each core, generated by flow across the abrupt permeability increase, plotted against the liquid and total pore volumes of injection.

Discussion

A series of injection rates and gas fractions were used to examine the effect of fractional flow and velocity on foam generation across a sharp permeability contrast of 3.8:1. Foam generation was observed at all the conditions tested. In computing foam apparent viscosity, if the pressure gradient remains the same, the computed apparent viscosity increases with decreasing velocity. While the experiment at $u_i = 0.17$ ft/d records the highest apparent viscosity, foam does not reach the outlet of the core, as reported in the previous section. Ignoring the experiment at the lowest velocity, Figure 7a shows that the measured pressure gradient is, for the most part, higher at a lower injection rate. This is counter-intuitive for two-phase flow but can be explained as follows: As capillary number (or velocity in this case, as permeability is kept constant) increases, the impact of capillary heterogeneity decreases (Yortsos & Chang, 1990). For the same reason, coreflooding experiments are often conducted at high injection rates in order to minimize the influence of the capillary end-effect. Therefore, as velocity in our experiments increases, the rate of foam generation may be affected in a way that the strength of the resulting foam is lower. Note that this would hold true only for foam created by snap-off across an abrupt increase in permeability. For other mechanisms of bubble generation, a higher velocity would lead to the creation of a stronger foam. From the results of our experiments it can be implied that a reduction in gas mobility can be expected far from wells in a foam EOR application, provided that sharp heterogeneities are present in the formation and injected surfactant and gas both reach the heterogeneity. For all practical purposes, it can be considered that this phenomenon is independent of velocity. While velocities as low as 0.17 ft/d may never be reached in a typical reservoir setting, we still observe foam generation across a permeability contrast

of 3.8:1 at this superficial velocity. At velocities much greater than 1 ft/d, other mechanisms of foam generation come into play and the impact of snap-off across heterogeneities may be less significant.

Experiments with varying gas fractions were conducted with the core placed horizontally on the CT scanner table. CT images together with pressure measurements were used to identify when foam generation began and whether foam successfully propagated towards the outlet of the core. Figure 13 shows a plot of the apparent viscosity in the high-permeability section plotted against pore volumes of surfactant solution injected for three different fractional flows. Once again, each point on the graph represents the average of all measurements recorded over a period of 0.05 liquid PVI (or 0.25 total PVI) and the error bar indicate the fluctuating nature of pressure gradient in that time interval. Since the total velocity and absolute permeability remains constant between the experiments, the trend in apparent viscosity also reflects the trend in pressure gradient in the high-permeability zone. The phase-saturation profiles corresponding to $f_g = 60\%$ and $f_g = 95\%$ are shown in Figure 10 and Figure 11, respectively. As discussed in the previous section, for the experiments conducted at $f_g = 80\%$ and $f_g = 95\%$, pressure gradient in the high-permeability zone rises before the CT images show a high gas saturation in that zone. Therefore, after approximately 0.1 PVI liquid, the apparent viscosity (μ_{app}^H) is circa 100 cP for these experiments (Figure 13). However, comparing the phase saturation profiles across the core, it can be seen that a foam front begins to develop and move through the high-permeability zone after roughly the same liquid volume has been injected. This observation is independent of f_g , and, as mentioned above, u_t . Moreover, the onset of foam generation is accompanied by fluctuations in pressure gradient, which are more frequent, and larger in magnitude in these two experiments compared to the test at $f_g = 60\%$. However, it takes longer (in terms of liquid PVI) for foam to propagate downstream to the outlet of the core at $f_g = 60\%$ compared to the other two experiments. In other words, it takes more surfactant solution for foam at 60% quality to travel the same distance as a foam at 95% quality.

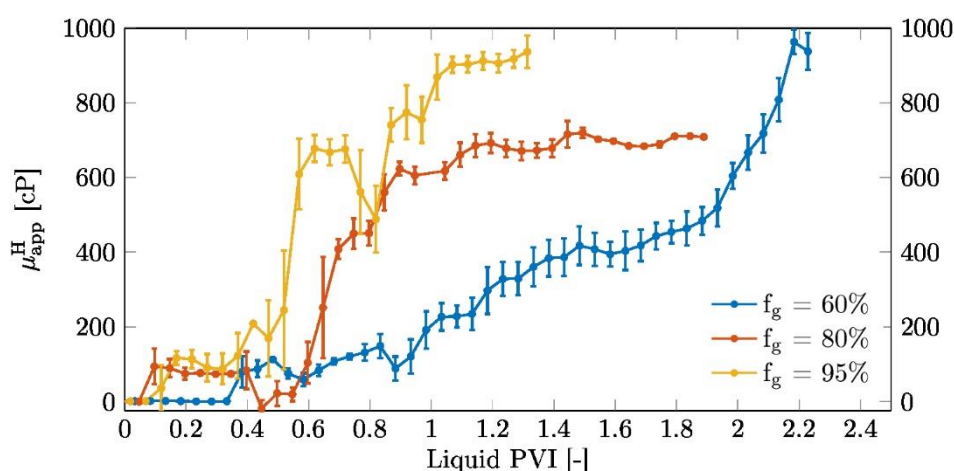


Figure 13 Apparent viscosity of foam in the high-permeability section of core 1 through experiments conducted at three different injected gas fractions with the core placed horizontally in the CT scanner. $u_t = 0.67$ ft/d in all the experiments.

At the end of the experiments shown in Figure 13 (and Figure 8), $\mu_{app}^H \approx 900$ cP for $f_g = 95\%$, 700 cP for $f_g = 80\%$, and 950 cP for $f_g = 60\%$. It is not entirely clear why the foam apparent viscosity drops at 80% foam quality. It is possible that if the experiment was continued for an extended period of time, the apparent viscosity would reach a similar value. Nevertheless, this observation is inconsistent with the observations of Tanzil et al. (2002) and Falls et al. (1988), who observed a decrease in pressure gradient and foam apparent viscosity with an increase in gas fraction. As mentioned in the “Introduction” section, in both their experiments, foam was generated across a permeability discontinuity as a combination of gas and surfactant solution drained a medium already saturated with surfactant solution. Moreover, in the experiments of Tanzil et al. (2002), a decrease in f_g between successive tests was also accompanied by an increase in u_t , since the gas velocity was kept constant.

These differences in experimental protocols may be responsible for the contrast in experimental observations. As Syukri (2018) performed so-called foam-quality-scan experiments (Ma et al., 2013, 2014) with a homogeneous sintered glass core with the same permeability as the high-permeability region of core 1. In his foam scans, foam was generated under drainage conditions by injecting gas and surfactant solution into a surfactant-saturated core. The transition foam quality was 80% and the foam apparent viscosity was lower at a foam quality of 60% and 95% compared to 80%. The experiments at $f_g = 60\%$ and $f_g = 95\%$ were performed again to ensure repeatability. The experiment at $f_g = 80\%$ and $u_t = 0.67$ ft/d is a replication of the experiment shown in Figure 12 (blue line). The results of all the experiments performed at the same injection conditions were similar and the discussion above holds, regardless of which experimental data we select.

In order to further investigate and validate the theory of foam generation across permeability contrasts by snap-off, we investigate the saturation profile in the core obtained through CT imaging, focusing on the permeability contrast. Figure 14 shows the average steady-state liquid saturation in the core plotted against dimensionless core length (x/L). Mean saturation values in the low- and high-permeability zones, and at the transition, are indicated by the dashed line. Every point on the graph represents average saturation inside a circular CT image slice along the length of the core. As mentioned earlier, the permeability jump in the core takes place over one, or at most two, “coarse” grain diameters, equivalent to circa 0.5 mm. Since the voxel depth (reported in Table 2) is more than this grain size, the CT measurement at the permeability contrast (at $x/L \approx 0.38$ in Figure 14) defines the average liquid saturation near the edge of the low-permeability zone. The exact liquid saturation one pore throat away from the heterogeneity can be higher. Nonetheless, the saturation profile gives a good indication of the behaviour across the heterogeneity in terms of liquid accumulation we can use this information to show a local reduction in capillary pressure at the edge of the low-permeability region.

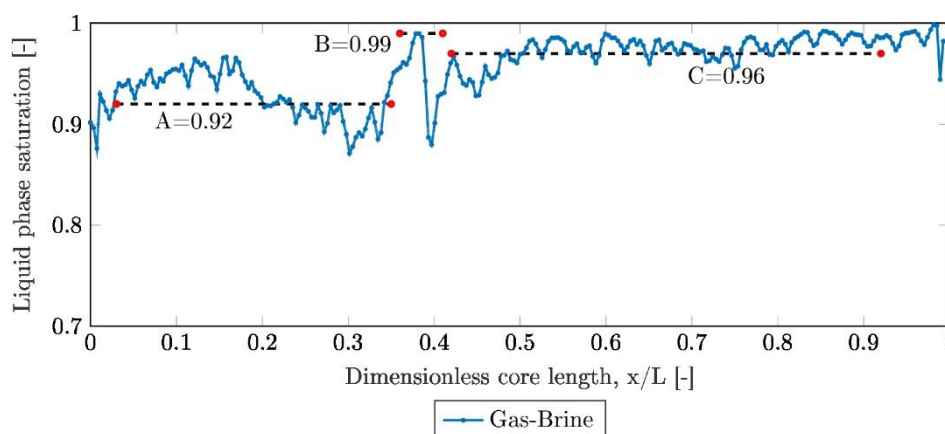


Figure 14 Steady-state liquid (brine) saturation across core 1 during gas-brine co-injection at the beginning of the experiment. Average saturations in the low-permeability zone, at the transition, and in the high-permeability zone are marked by the dashed lines.

Berg et al. (2014) and Armstrong et al. (2016) measured capillary pressure as a function of saturation using mercury-intrusion porosimetry for sintered glass core plugs, as used in this study. We use the Leverett-J function Leverett (1941) to extend these measurements to the petrophysical properties of core 1 and fluid properties of our two-phase system, and construct capillary-pressure curves for the two regions in the core. The curves are plotted on a semi-log scale in Figure 15. As indicated in the figure, capillary-pressure curves obtained through mercury-intrusion porosimetry include an entry-slope region. Several authors have investigated the physical meaning of this region (Katz & Thompson, 1986; Nabawy, Géraud, Rochette, & Bur, 2009; Schowalter, 1979). The entry-slope region concerns pore throats near the edges of the porous medium that are being entered by the non-wetting phase. It is not representative of drainage in the bulk of the porous medium. Therefore, we estimate the capillary entry pressure of the low-permeability zone by extending the P_c curve (ignoring the entry-slope region) to intersect with the vertical line representing a water-saturated core ($S_w=1$),

indicated by the dashed arrow in Figure 15a. Note that to model snap-off, however, imbibition-type capillary pressure curves must be used (Falls et al., 1988) which include the entry-slope region. Drainage capillary pressure curves do not allow for snap-off since P_c is always higher than P_c^e , anywhere on the curve. In Figure 15b, the curve is expanded close to the liquid-saturated end. The average liquid saturations indicated in Figure 14 are plotted on the curve. $P_c^{sn}/P_c^e=1/2$ is assumed (Falls et al., 1988) and marked by the green dashed line on the plot. The capillary pressure corresponding to the average saturation in the low-permeability zone (A) is just above the entry pressure of the region. At the transition, liquid accumulates to maintain capillary continuity and it can be seen that the capillary pressure drops to below the capillary pressure for snap-off (B). The capillary pressure corresponding to the average liquid saturation in the high-permeability zone is close to P_c at the transition. In alignment with the theory of Yortsos & Chang (1990), this response indicates that the permeability contrast is sharp and monotonic. Moreover, since P_c at the transition is lower than P_c^{sn} , snap-off is observed as surfactant is introduced into the system. This is consistent with the work of Rossen (1999) and Falls et al. (1988). A similar investigation can be followed in all the experiments performed with CT-assisted saturation measurements. It is observed that capillary pressure at the boundary of the low-permeability zone drops below the critical capillary pressure for snap-off, resulting in foam generation across the permeability contrast. A complete analysis of the path followed along the P_c curve would include the edge effect on the measured drainage capillary pressure curves in Figure 15 and the effect of imbibition on the low-permeability section at the boundary.

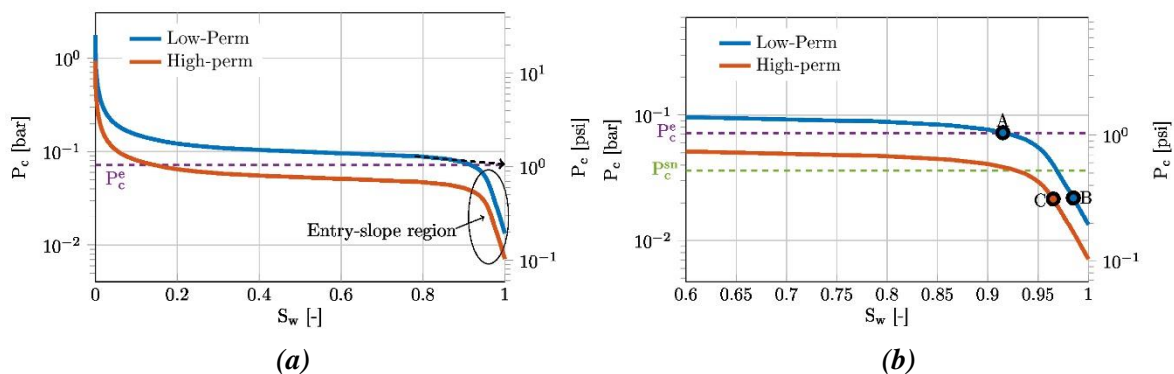


Figure 15 Capillary pressure curves for the high- and low-permeability regions in the core extracted from the measurements of Berg et al. (2014) and adjusted to the petrophysical properties of core 1 and the fluid properties of our two-phase system (a); capillary pressure corresponding to average liquid saturations indicated in Figure 14 (b).

Conclusion

Experiments at low superficial velocities were conducted with a variety of fractional flows in a layered core to observe foam generation by snap-off. In a petroleum reservoir, ten metres away from the injection well, fluid velocity can be as much as 100 times lower than that in the immediate vicinity of the well. As a result, foam strength can be significantly lower and foam propagation may fail (Ashoori et al., 2012; Friedmann et al., 1994). The results of this study show that if the geological setting allows for the presence of sharp changes in permeability in a reservoir, snap-off can help reduce gas mobility away from wells where the superficial velocities are low. These heterogeneities can exist in the form of layer boundaries or laminations and cross-laminations within individual layers, with the former exhibiting contrasts often larger than those considered in this study. The permeability changes can be parallel or perpendicular to the direction of flow, or a combination of the two. When the contrast is parallel to the direction of flow, upward migration of gas due to gravity can cause foam generation in the high-permeability layers. Once foam is generated, gas mobility in the vertical direction will be reduced, effectively increasing the segregation length (Stone, 1982; Jenkins, 1984; Rossen and van Duijn, 2004) and improving sweep efficiency in the low-permeability layers. In the presence of lateral changes in permeability, snap-off may help maintain foam strength and improve the mobility control deep inside the formation. Foam generation across sharp permeability

contrasts can have important consequences for foam EOR applications and it must be accounted for to account for the improvement in overall sweep efficiency.

In this study, foam generation was observed almost immediately once the surfactant solution arrived at the permeability contrast, irrespective of f_g or u_i . However, when the permeability contrast was greater, a larger amount of liquid was injected before foam was observed in the high-permeability zone. Note that in our synthetic porous medium surfactant adsorption is almost negligible. In realistic subsurface setting, adsorption must first be satisfied before foam generation commences. In agreement with the observations of Falls et al. (1988), snap-off across the permeability contrast was an intermittent process. This is best indicated by periods of fluctuating pressure gradient that mark the onset of foam generation and subsequent propagation. This intermittency, in terms of magnitude and frequency of fluctuations in pressure gradient, was greater at greater permeability contrasts, higher gas fractions and lower velocities. The saturation maps constructed using CT imaging for some of our experiments helped confirm that foam was indeed generated at the permeability transition and from there on it propagates downstream to the end of the core. The saturation were also used to show that the local reduction in capillary pressure near the permeability jump is consistent with previous theory (Falls et al., 1988; Yortsos and Chang, 1990; Rossen, 1999).

Acknowledgements

This paper is a result of the collaboration between Delft University of Technology and Universiti Teknologi PETRONAS. We thank PETRONAS and Shell for funding this research. We gratefully acknowledge Michiel Slob, Ellen Meijvogel-de Koning, Marc Friebe, Karel Heller, Joost van Meel and Jolanda van Haagen-Donker for their extensive technical support at the Laboratory of Geoscience and Engineering of Delft University of Technology.

References

- Armstrong, R. T., McClure, J. E., Berrill, M. A., Rücker, M., Schlüter, S., & Berg, S. (2016). Beyond Darcy's Law: The Role of Phase Topology and Ganglion Dynamics for Two-Fluid Flow. *Phys. Rev. E*, 94(043113). [doi: 10.1103/PhysRevE.94.043113](https://doi.org/10.1103/PhysRevE.94.043113)
- As Syukri, H. (2018). *Experimental Study: Foam Generation and Propagation in Flow Across a Permeability Contrast*. Delft University of Technology, Delft, The Netherlands. [uuiid: 961bf2b5-28d5-41e4-9283-a20e1c5d672b](https://www.researchgate.net/publication/328541e4-9283-a20e1c5d672b)
- Ashoori, E., Marchesin, D., & Rossen, W. R. (2012). Multiple Foam States and Long-Distance Foam Propagation in Porous Media. *SPE J.*, 17(04), 1231–1245. [doi: 10.2118/154024-PA](https://doi.org/10.2118/154024-PA)
- Berg, S., Armstrong, R., Ott, H., Georgiadis, A., Klapp, S. A., Schwing, A., ... Stampanoni, M. (2014). Multiphase Flow in Porous Rock Imaged Under Dynamic Flow Conditions with Fast X-Ray Computed Microtomography. *Petrophysics*, 55(04), 304–312.
- Chambers, D. J. (1994). Foams for Well Stimulation. In L. L. Schramm (Ed.), *Foams: Fundamentals and Applications in the Petroleum Industry* (Vol. 242, pp. 355–404). American Chemical Society. [doi: 10.1021/ba-1994-0242.ch009](https://doi.org/10.1021/ba-1994-0242.ch009)
- Chambers, K., & Radke, C. J. (1990). Capillary Phenomena in Foam Flow through Porous Media. In N. R. Morrow (Ed.) (Vol. 36). Marcel Dekker, Inc.
- Dake, L. P. (1994). *The Practice of Reservoir Engineering* (Vol. 36). Amsterdam: Elsevier.
- Falls, A. H., Hirasaki, G. J., Patzek, T. W., Gauglitz, D. A., Miller, D. D., & Ratulowski, T. (1988). Development of a Mechanistic Foam Simulator: The Population Balance and Generation by Snap-Off. *SPE Reserv. Eng.*, 3(03), 884–892. [doi: 10.2118/14961-PA](https://doi.org/10.2118/14961-PA)
- Farajzadeh, R., Krastev, R., & Zitha, P. L. J. (2008). Foam Films Stabilized with Alpha Olefin Sulfonate (AOS). *Colloids Surfaces A Physicochem. Eng. Asp.*, 324(1–3), 35–40. [doi: 10.1016/J.COLSURFA.2008.03.024](https://doi.org/10.1016/J.COLSURFA.2008.03.024)
- Friedmann, F., Chen, W. H., & Gauglitz, P. A. (1991). Experimental and Simulation Study of High-Temperature Foam Displacement in Porous Media. *SPE Reserv. Eng.*, 6(01), 37–45. [doi: 10.2118/17357-PA](https://doi.org/10.2118/17357-PA)
- Friedmann, F., Smith, M. E., Guice, W. R., Gump, J. M., & Nelson, D. G. (1994). Steam-Foam

- Mechanistic Field Trial in the Midway-Sunset Field. *SPE Reserv. Eng.*, 9(04), 297–304. [doi: 10.2118/21780-PA](https://doi.org/10.2118/21780-PA)
- Gauglitz, P. A., Friedmann, F., Kam, S. I., & Rossen, W. R. (2002). Foam generation in homogeneous porous media. *Chem. Eng. Sci.*, 57(19), 4037–4052. [doi: 10.1016/S0009-2509\(02\)00340-8](https://doi.org/10.1016/S0009-2509(02)00340-8)
- Gupta, D. V. S. (2009). Unconventional Fracturing Fluids for Tight Gas Reservoirs. In *SPE-119424-MS*. Presented at the SPE Hydraulic Fracturing Technology Conference, The Woodlands, Texas, 19-21 January. [doi: 10.2118/119424-MS](https://doi.org/10.2118/119424-MS)
- Hartkamp-Bakker, C. A. (1993). *Permeability heterogeneity in cross-bedded sandstones: Impact on water/oil displacement in fluvial reservoirs*. Delft University of Technology. [uiid: be8ffa8f-5b66-4c46-932b-56d3eab5823e](https://uiid:be8ffa8f-5b66-4c46-932b-56d3eab5823e)
- Hirasaki, G. J., Jackson, R. E., Jin, M., Lawson, J. B., Londergan, J., Meinardus, H., ... Tanzil, D. (2000). Description of Surfactant/Foam Process and Surfactant-Enhanced Aquifer Remediation. In S. Fiorenza, C. A. Miller, C. L. Oubre, & C. H. Ward (Eds.), *NAPL Removal: Surfactants, Foams, and Microemulsions* (pp. 7–10). Boca Raton: CRC Press. [doi: 10.1201/9781420026207.pt1](https://doi.org/10.1201/9781420026207.pt1)
- Hirasaki, G. J., Miller, C. A., Szafranski, R., Tanzil, D., Lawson, J. B., Meinardus, H., ... Wade, W. H. (1997). Field Demonstration of the Surfactant / Foam Process for Aquifer Remediation. *Society of Petroleum Engineers*, (October 2015). [doi: 10.2118/39292-MS](https://doi.org/10.2118/39292-MS)
- Kahrobaei, S., Vincent-Bonnieu, S., & Farajzadeh, R. (2017). Experimental Study of Hysteresis Behavior of Foam Generation in Porous Media. *Sci. Reports*, 7(1), 8986. [doi: 10.1038/s41598-017-09589-0](https://doi.org/10.1038/s41598-017-09589-0)
- Kam, S. I., & Rossen, W. R. (2003). A Model for Foam Generation in Homogeneous Media. *SPE J.*, 8(4), 417–425. [doi: 10.2118/87334-PA](https://doi.org/10.2118/87334-PA)
- Katz, A. J., & Thompson, A. H. (1986). Quantitative Prediction of Permeability in Porous Rock. *Phys. Rev. B*, 34(11), 8179–8181. [doi: 10.1103/PhysRevB.34.8179](https://doi.org/10.1103/PhysRevB.34.8179)
- Kovscek, A. R., & Radke, C. J. (1994). Fundamentals of Foam Transport in Porous Media. In L. L. Schramm (Ed.) (Vol. 242, pp. 115–163). Washington, DC: American Chemical Society. [doi: 10.1021/ba-1994-0242.ch003](https://doi.org/10.1021/ba-1994-0242.ch003)
- Lake, L. W., Johns, R.T., Rossen, W.R., & Pope, G. (2014). *Fundamentals of Enhanced Oil Recovery*. Richardson, Texas: Society of Petroleum Engineers.
- Lenormand, R., Zarcone, C., & Sarr, A. (1983). Mechanisms of the Displacement of One Fluid by Another in a Network of Capillary Ducts. *J. Fluid Mech.*, 135, 337–353. [doi: 10.1017/S0022112083003110](https://doi.org/10.1017/S0022112083003110)
- Leverett, M. C. (1941). Capillary Behavior in Porous Solids. *Transactions of the AIME*, 142(01), 152–169. [doi: 10.2118/941152-G](https://doi.org/10.2118/941152-G)
- Li, Q., & Rossen, W. R. (2005). Injection Strategies for Foam Generation in Homogeneous and Layered Porous Media. Presented at the SPE Annual Technical Conference and Exhibition, Dallas, Texas, 9-12 October. [doi: 10.2118/96116-MS](https://doi.org/10.2118/96116-MS)
- Lyons, W. C., Guo, B., Graham, R. L., & Hawley, G. D. (2009). *Air and Gas Drilling Manual (Third Edition)*. Gulf Professional Publishing. [doi: 10.1016/B978-0-12-370895-3.X0001-6](https://doi.org/10.1016/B978-0-12-370895-3.X0001-6)
- Ma, K., Farajzadeh, R., Lopez-Salinas, J. L., Miller, C. A., Biswal, S. L., & Hirasaki, G. J. (2014). Non-uniqueness, Numerical Artifacts, and Parameter Sensitivity in Simulating Steady-State and Transient Foam Flow Through Porous Media. *Transp. Porous Media*, 102(3), 325–348. [doi: 10.1007/s11242-014-0276-9](https://doi.org/10.1007/s11242-014-0276-9)
- Ma, K., Lopez-Salinas, J. L., Puerto, M. C., Miller, C. A., Biswal, S. L., & Hirasaki, G. J. (2013). Estimation of Parameters for the Simulation of Foam Flow through Porous Media. Part 1: The Dry-Out Effect. *Energy Fuels*, 27(5), 2363–2375. [doi: 10.1021/ef302036s](https://doi.org/10.1021/ef302036s)
- McCool, C. S., Parmeswar, R., & Willhite, G. P. (1983). Interpretation of Differential Pressure in Laboratory Surfactant/Polymer Displacements. *SPE J.*, 23(05), 791–803. [doi: 10.2118/10713-PA](https://doi.org/10.2118/10713-PA)
- Mees, F., Swennen, R., & Geet, M. Van. (2003). Applications of X-ray Computed Tomography in the Geosciences. *Geological Society*,. Geol. Soc. Special Publication 215, 1–6. [doi: 10.1144/GSL.SP.2003.215.01.01](https://doi.org/10.1144/GSL.SP.2003.215.01.01).
- Nabawy, B. S., Géraud, Y., Rochette, P., & Bur, N. (2009). Pore-throat Characterization in Highly Porous and Permeable Sandstones. *Am. Assoc. Pet. Geol. Bull.*, 93(6), 719–739.

[doi: 10.1306/03160908131](https://doi.org/10.1306/03160908131)

- Reineck, H. E., & Singh, J. B. (1980). *Depositional Sedimentary Environments*. Berlin, Heidelberg: Springer Berlin Heidelberg. [doi: 10.1007/978-3-642-96291-2](https://doi.org/10.1007/978-3-642-96291-2)
- Rossen, W. R. (1996). Foams in Enhanced Oil Recovery. In R. K. Prud'homme & S. A. Khan (Eds.), *Foams: Theory, Measurements and Applications* (Vol. 57, pp. 413–464). New York: Marcel Dekker. [doi: 10.1201/9780203755709](https://doi.org/10.1201/9780203755709)
- Rossen, W. R. (1999). Foam Generation at Layer Boundaries in Porous Media. *SPE J.*, 4(04), 409–412. [doi: 10.2118/59395-PA](https://doi.org/10.2118/59395-PA)
- Rossen, W. R. (2003). A Critical Review of Roof Snap-Off as a Mechanism of Steady-State Foam Generation in Homogeneous Porous Media. *Colloids Surfaces A: Physicochem. Eng. Asp.*, 225(1–3), 1–24. [doi: 10.1016/S0927-7757\(03\)00309-1](https://doi.org/10.1016/S0927-7757(03)00309-1)
- Rossen, W. R., & Gauglitz, P. A. (1990). Percolation theory of creation and mobilization of foams in porous media. *AIChE J.*, 36(8), 1176–1188. [doi: 10.1002/aic.690360807](https://doi.org/10.1002/aic.690360807)
- Schindelin, J., Arganda-Carreras, I., Frise, E., Kaynig, V., Longair, M., Pietzsch, T., ... Cardona, A. (2012). Fiji: An Open-source Platform for Biological-image Analysis. *Nat. Methods*, 9(7), 676–682. [doi: 10.1038/nmeth.2019](https://doi.org/10.1038/nmeth.2019)
- Schowalter, T. T. (1979). Mechanics of Secondary Hydrocarbon Migration and Entrapment. *AAPG Bulletin*, 5(0149), 723–760. [doi: 10.1306/2F9182CA-16CE-11D7-8645000102C1865D](https://doi.org/10.1306/2F9182CA-16CE-11D7-8645000102C1865D)
- Shah, S. Y., Wolf, K.-H., Pilus, R., & Rossen, W. R. (2018). Foam Generation by Capillary Snap-off in Flow Across a Sharp Permeability Transition. *SPE Journal* (in press; posted 31 December 2018). [doi: 10.2118/190210-PA](https://doi.org/10.2118/190210-PA).
- Tanzil, D., Hirasaki, G. J., & Miller, C. A. (2002). Conditions for Foam Generation in Homogeneous Porous Media. Presented at the SPE/DOE Improved Oil Recovery Symposium, Tulsa, Oklahoma, 13-17 April. [doi: 10.2118/75176-MS](https://doi.org/10.2118/75176-MS)
- Tanzil, D., Hirasaki, G. J., & Miller, C. A. (2002). Mobility of Foam in Heterogeneous Media: Flow Parallel and Perpendicular to Stratification. *SPE Journal*, 7(02), 203–212. [doi: 10.2118/78601-PA](https://doi.org/10.2118/78601-PA)
- Yang, J., & Siddiqui, S. (1999). The Use Of Foam To Improve Liquid Lifting From Low-Pressure Gas Wells. In *PETSOC-99-126*. Presented at the Petroleum Conference of The South Saskatchewan Section, Regina, Saskatchewan, October 18 - 21. [doi: 10.2118/99-126](https://doi.org/10.2118/99-126)
- Yortsos, Y. C., & Chang, J. (1990). Capillary Effects in Steady-state Flow in Heterogeneous Cores. *Transp. Porous Media*, 5(4), 399–420. [doi: 10.1007/BF01141993](https://doi.org/10.1007/BF01141993)
- Yu, G., Vincent-Bonnieu, S., Rossen, W. R. (2018). Foam Propagation at Low Superficial Velocity: Implications for Long-Distance Foam Propagation. Presented at the EAGE Improved Oil recovery Conference, Pau, France, April 8-11.